CHIN.PHYS.LETT. Vol. 18, No. 1 (2001) 68

Space Environment Simulation for Material Processing by Acoustic Levitation *

XIE Wen-Jun(解文军), WEI Bing-Bo(魏炳波)
Department of Applied Physics, Northwestern Polytechnical University, Xi'an 710072

(Received 14 April 2000)

Single-axis acoustic levitation of four polymer samples has been realized in air under the ground-based laboratory conditions for the purpose of space environment simulation of containerless processing. The levitation capabilities are investigated by numerical calculations based on a model of the boundary element method corresponding to our levitator and following Gor'kov and Barmatz's method. The calculated results, such as the resonant distance between the reflector and the vibrating source and the positions of levitated samples, agree well with experimental observation, and the effect of gravity on the time-averaged potential for levitation force is also revealed. As an application, the containerless melting and solidification of a liquid crystal, 4-Pentylphenyl-4'-methybenzoate, is successfully accomplished, in which undercooling up to 16 K is obtained and the rotation and oscillation of the sample during solidification may result in fragmentation of the usual radiating surface growth morphology.

PACS: 43. 25. Uv, 81. 20. Zx

The outer space environment provides some unique conditions for material research, such as containerless processing of materials which has aroused special research interest because it avoids the contamination of samples from container walls.[1,2] Acoustic levitation has been an important technique used for positioning samples in space and now becomes a promising method for space environment simulation of containerless processing under ground-based conditions.[3,4] Its applications include undercooling liquids, measuring thermodynamic properties, and studying fluid dynamics of free drops and bubbles.[5−9] The advantage of the acoustic method is its applicability to dielectric materials and low melting-point metallic materials. This letter reports the new results of acoustic containerless processing, its numerical analysis and its application to melting and solidification of a liquid crystal.

In our previous work, a single-axis acoustic levitator has been built up.[10,11] The major part of the levitator includes a vibrating source with a frequency of 16.7 kHz and a reflector with a carved surface facing it, as shown in Fig. 1. The vibrating source–reflector axis is parallel to the direction of gravity and a standing acoustic wave is generated along this direction to counteract the gravitational force acting on the samples. The distance between the reflector and the vibrating source can be adjusted to produce a certain resonant mode of the acoustic field. For example, a mode with four force potential wells in air is shown in Fig. 1. The surface of the reflector is designed in a concave shape because it improves the capabilities of levitation as compared with a planar one.

In terrestrial studies of the acoustic levitation, much attention was paid to the ability and stability of the acoustic field. Gor'kov[12] and Barmatz *et al.*[13,14] have performed useful theoretical studies on this problem by analysing plane standing waves and some simple fields, such as that constrained by rectangular, cylindrical and spherical chambers. However, for a practical levitator as described in this letter, more accurate analysis is needed. Our analysis follows the method developed by Gor'kov and Barmatz *et al.*, which defines a time-averaged potential $U_{\rm a}$ for the acoustic radiation force acting on a small rigid spherical sample in an arbitrary acoustic field in an ideal fluid:

$$U_{\rm a} = 2\pi R_{\rm s}^3 \left(\frac{\overline{p_{\rm in}^2}}{3\rho_{\rm f} c^2} - \frac{\rho_{\rm f} \overline{\boldsymbol{v}_{\rm in}^2}}{2} \right), \tag{1}$$

where $\overline{p_{\rm in}^2}$ and $\overline{\boldsymbol{v}_{\rm in}^2}$ are the mean square fluctuations of the incident pressure and velocity at the point where the sample with radius $R_{\rm s}$ is located, $\rho_{\rm f}$ is the density of the fluid, and c is the sound speed.

To include the gravitational force, a corresponding potential $U_{\rm g}$ is also defined:

$$U_{\rm g} = (m_{\rm s} - m_{\rm f}) g h, \tag{2}$$

where $m_{\rm s}$ is the mass of the sample, $m_{\rm f}$ is the mass of the fluid displaced by the sample, h is the perpendicular position of the sample and g is the gravitational acceleration. Thus the total potential is the sum of the acoustic term and the gravitational term:

$$U = U_{\rm a} + U_g. \tag{3}$$

From the above three equations, the force on the sample, the levitation positions and the restoring force constants will be derived by the differentiation of the potential U, which makes a quantitative evaluation of the levitation capabilities accessible.[13]

* Supported by the National Natural Science Foundation of China under Grant No. 59871040, and the National High Technology Development Program of China under Grant No. 863-2-4-3-2.

©2001 Chinese Physical Society and IOP Publishing Ltd

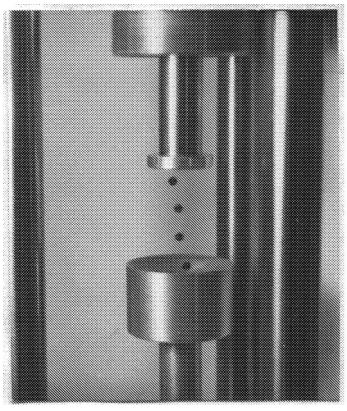


Fig. 1. Single-axis acoustic levitation of four polymer samples with a diameter of 3 mm.

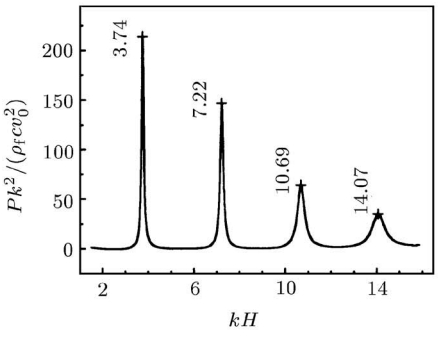


Fig. 2. Dimensionless acoustic radiation power versus dimensionless distance between reflector and vibrating source. The peaks correspond to resonant modes of the acoustic field.

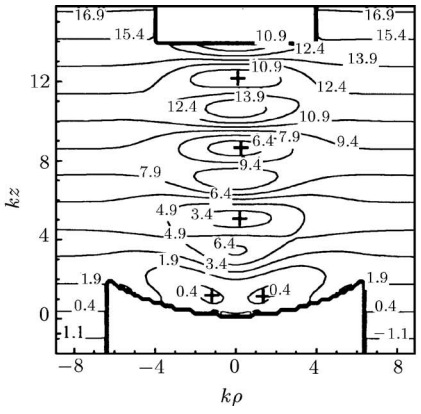


Fig. 3. Contour of dimensionless time-averaged potential $U/(2\pi\rho_f v_0^2 R_s^3)$ with $v_0 = 4\,\mathrm{m/s}$, $\rho_s/\rho_f = 826.4$ and $g = 9.8\,\mathrm{m{\cdot}s^{-2}}$. The symbol "+" denotes the potential well.

So far the problem is how to calculate the incident pressure and velocity. We simplify the acoustic levitator into two coaxial cylinders of which the upper one is the sound source with its underside as the vibrating surface and the lower one is the reflector with a concave upside as the reflecting surface. The gravitational force is downwards along the cylindrical axis. The incident acoustic field can be described as the boundary integral over the surfaces of these two cylinders as written in Eq. 4 and then numerically computed by the boundary element method:

$$C(M)\Phi(M) = \int_\Gamma \left[\frac{\partial \Phi(Q)}{\partial n} \frac{\exp(\mathrm{j}kr)}{4\pi r} - \Phi(Q) \frac{\partial}{\partial n} \left(\frac{\exp(\mathrm{j}kr)}{4\pi r} \right) \right] \mathrm{d}\Gamma(Q), \tag{4}$$

where M is an arbitrary point in space, Q an arbitrary point at the surface Γ with unit outward normal n, r is the distance between M and Q, k is the wave number, and C is a constant related to the geometric property at the point M. Here Φ is the incident velocity potential from which the incident pressure p_{in} and velocity $\boldsymbol{v}_{\mathrm{in}}$ will be easily obtained by the differentiation of Φ with respect to time and space, respectively.

During the calculation all the quantities are made dimensionless. For example, the dimensionless length is kx, the dimensionless velocity is $\boldsymbol{v}/v_0$, and the dimensionless pressure is $p/(\rho_f c v_0)$. Here v_0 is the velocity amplitude of the vibrating source.

Generally, single-axis acoustic levitation works at the resonant states of the acoustic field to achieve the largest acoustic radiating force. In order to find the distance between the reflector and the vibrating source at which the acoustic field reaches a certain resonant mode, the profile of the dimensionless acoustic radiation power $Pk^2/(\rho_f c v_0^2)$ versus the distance kH is calculated as shown in Fig. 2. There are four peaks in the profile and each of them denotes a resonant mode. To compare with the experiment shown in Fig. 1, the geometric parameters are taken to be the same as those in experiment and the fourth mode is further studied, which shows a resonant distance of $kH = 14.07$. As to air at room temperature, $k = 0.309\,\mathrm{mm^{-1}}$, the prediction of the resonant distance of $H = 45.6\,\mathrm{mm}$ is instantly obtained which is in close agreement with the measured value of 44.3 mm.

The distribution of the time-averaged potential U in the dimensionless form of $U/(2\pi\rho_f v_0^2 R_s^3)$ is plotted in Fig. 3. It shows four potential minima, of which each denotes a possible position for levitation. The upper three minima are the points at the symmetric axis and the lower one is a circle around the symmetric axis. This circle-type potential well explains why the sample near the reflector deviates from the symmetric axis. Compared with Fig. 1, it can be seen that the calculated potential wells are in close agreement with levitation positions observed in the experiment, except for the upper one. The deviation of the sample near the vibrating source may have resulted from the complication of the vibration form. In our calculation the vibrating source is simplified as a piston.

The effect of the gravitational level on the time-averaged potential and the total force along the symmetric axis are shown in Figs. 4 and 5, respectively. For Fig. 4, the gravitational level changes the depth of the potential wells and the positions of the samples. At zero gravity, which is close to the space micro-gravitational condition, the potential wells are the deepest. With the increase of the gravitational level, the potential wells become shallower and some of them even disappear, and at the same time the positions of samples are lowered until some of the samples fall to the reflector. Since the gravitational force is a constant, the profile of the total force is simply shifted downwards as the gravitational acceleration increases, as shown in Fig. 5. It can be seen that at unit gravity the maximum total force near $kz = 4$ is below zero,

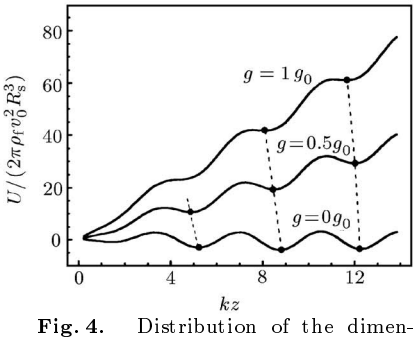


Fig. 4. Distribution of the dimensionless time-averaged potential along the cylindrical axis at different gravitational levels. Here $v_0 = 1.8\,\mathrm{m/s}$, $\rho_s/\rho_f = 826.4$ and $g_0 = 9.8\,\mathrm{m{\cdot}s^{-2}}$.

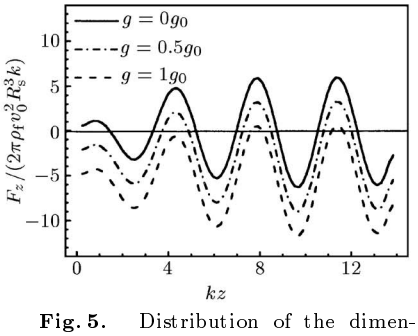


Fig. 5. Distribution of the dimensionless total force along the cylindrical axis at different gravitational levels. Here $v_0 = 1.8\,\mathrm{m/s}$, $\rho_s/\rho_f = 826.4$ and $g_0 = 9.8\,\mathrm{m{\cdot}s^{-2}}$.

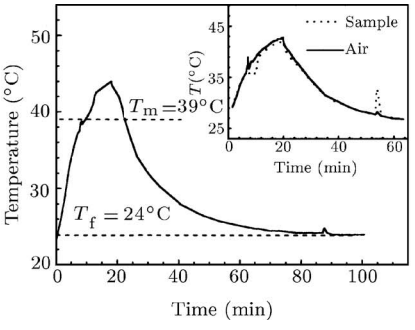


Fig. 6. Profile of heating and cooling of an acoustic levitated liquid crystal.

which means the gravitational force is larger than the acoustic force and hence the sample at this location will not be levitated. To produce a large enough acoustic force to balance the gravity, one can increase the vibrating strength v_0 or decrease the ratio of ρ_s/ρ_f. For example, the potential well at this location reappears when $v_0 = 4\,\mathrm{m/s}$, as shown in Fig. 3.

As an application to containerless processing of materials by acoustic levitation, an attempt has been made on the melting and solidification of a liquid crystal, 4-Pentylphenyl-4'-methybenzoate. This is a thermotropic liquid crystal with monotropic phase transitions. Its melting point and clear point are 36°C and 12°C, respectively. The sample with $\sim 4\,\mathrm{mm}$ in diameter is levitated at the lowest-order mode that corresponds to the first peak in Fig. 2, and is then heated by hot air and cooled naturally to perform melting and solidification. Because the heating and cooling of air will increase and decrease the wavelength, respectively, the distance between the reflector and the vibrating source is adjusted correspondingly during heating and cooling processing to keep the resonance of the acoustic field. The temperature is detected by an NiCr–NiSi thermocouple with its tip about 2 mm near the sample. A typical record of temperature history is shown in Fig. 6, which gives a melting temperature of 39°C and a solidification temperature of 24°C. In fact, the temperature detected is that of the air near the sample. The difference in temperatures between the sample and the air is also shown in Fig. 6. It indicates that the difference is almost negligible except for the melting and solidification stages where the temperatures of the air are about 3°C higher and 5°C lower than those of the sample, respectively. The undercooling in Fig. 6 is 12 K. In our experiment undercooling up to 16 K has been obtained.

The shape of samples is close to a sphere before melting and becomes pancake-like after melting because the force exerted in the perpendicular direction is much larger than that in horizontal directions. When the liquid is solidified, the pancake-like shape is reserved. On the surface of the solidified samples radiating growth morphology can be observed which is similar to that formed under usual conditions. However, there also exists some fragmentation of this radiating surface growth morphology, which may be a result of the rotation and oscillation of the levitated sample during solidification.

In conclusion, single-axis acoustic levitation of four polymer samples with 3 mm diameters has been carried out to simulate the space environment for containerless processing on Earth. The capabilities of levitation are calculated by the boundary element method, and the prediction of resonant distances between the reflector and the vibrating source and positions of levitated samples agree well with the experimental observation. The effects of the gravitational level on the time-averaged potential and the levitation force are discussed. The increase of the gravitational acceleration leads to the decrease of the depth of potential wells. In addition, application of the acoustic levitation to containerless melting and solidification of a liquid crystal is accomplished during which undercooling up to 16 K is obtained and the sample rotation and oscillation may result in fragmentation of the usual radiating growth morphology on the sample surface.

REFERENCES

[1] Brandt E H 1989 *Science*, **24** 349
[2] Willnecker R et al 1986 *Appl. Phys. Lett.* **49** 1339
[3] Whymark R R et al 1979 *AIAA Paper* No. 79-0320
[4] Trinh E H 1995 *Rev. Sci. Instrum.* **56** 2059
[5] Ohsaka K et al 1990 *J. Cryst. Growth*, **106** 191
[6] Ansell S et al 1997 *Phys. Rev. Lett.* **78** 464
[7] Trinh E H and Ohsaka K 1995 *Int. J. Thermophys.* **16** 545
[8] Wang T G et al 1986 *Phys. Rev. Lett.* **56** 452
[9] XIE Z X et al 1998 *Chin. Phys. Lett.* **15** 813
[10] Xie W J et al 1999 *Acta Phys. Sin.* **48** 250 (in Chinese)
[11] Gao J R et al 1998 *Chin. J. Aeronautics*, **11** 228
[12] Gor'kov L P 1962 *Sov. Phys. Dokl.* **6** 773
[13] Barmatz M and Collas P 1985 *J. Acoust. Soc. Am.* **77** 928
[14] Collas P et al 1989 *J. Acoust. Soc. Am.* **86** 777